4670 *Inorg. Chem.* **2010**, *49*, 4670–4680
DOI: 10.1021/ic100486g

Inorganic Chemistry
Article

La_4LiAuO_8 and La_2BaPdO_5: Comparing Two Highly Stable d^8 Square-Planar Oxides

Joshua A. Kurzman, Xiaoying Ouyang, Won Bin Im, Jun Li, Jerry Hu, Susannah L. Scott,* and Ram Seshadri*

Department of Chemistry and Biochemistry, Department of Chemical Engineering, Materials Department, and Materials Research Laboratory, University of California, Santa Barbara, California 93106

Received March 13, 2010

La_4LiAuO_8 and La_2BaPdO_5, two previously known oxides, are presented as model compounds for examining the role of isolated and immobilized Au^{3+} and Pd^{2+} ions in heterogeneous catalysis. Structural characterization, stability, surface composition, and electronic structure of these compounds are presented. These are examined in studies ranging from synchrotron X-ray scattering, including pair distribution function (PDF) and maximum entropy method (MEM) analysis, to density functional calculations of the electronic structures. The exceptional stability displayed by these compounds as verified by thermogravimetric analysis can be attributed to the presence of covalent Au−O and Pd−O interactions revealed in MEM studies, which suggests a criterion for stabilizing these highly oxophobic transition metals in oxide environments. Catalytic testing of the two compounds as heterogeneous catalysts in the oxidation of CO to CO_2 are presented. La_2BaPdO_5 appears to be an effective catalyst for CO oxidation, despite the low surface area of the oxide being used. This is the first time that a fully ordered (rather than doped) Pd^{2+} oxide had been used to catalyze CO oxidation. La_4LiAuO_8 on the other hand, is much less effective at catalyzing CO oxidation. Differences in the reactivities of the two compounds are discussed with respect to differences in their density functional electronic structures.

Introduction

There is increasing evidence pointing to the importance of noble metal ions, particularly Pd^{2+}, Pt^{2+}, and Pt^{4+} in heterogeneous catalysis,[1−7] and that too in systems where it has been long believed that the catalysis took place on zerovalent metals (nanoparticles). In the case of Au, although it is now well established that nanoparticulate gold is catalytically active,[8,9] the precise identity of the active species, and the possibility of multiple active sites working in synergy, remains an area of active investigation.[10] Ascertaining which gold species are active—whether zerovalent nanoparticles or charged Au ions—has been particularly challenging, and is a crucial component of being able to understand the underlying mechanisms in heterogeneous catalysis by gold. Results in the literature are somewhat conflicting.[11−21] The choice of support is clearly intimately tied to the catalytic activity of nanoparticulate gold, but the plethora of interactions that can occur between gold and the support present significant difficulties in modeling such systems.[14] Considering the minute amounts of ionic Au in many of the catalytic systems investigated, untangling the identity of the active species is an ongoing problem. In the light of these observations, we

*To whom correspondence should be addressed. E-mail: sscott@engineering.ucsb.edu (S.L.S.), seshadri@mrl.ucsb.edu (R.S.).

(1) Priolkar, K. R.; Bera, P.; Sarode, P. R.; Hegde, M. S.; Emura, S.; Kumashiro, R.; Lalla, N. P. *Chem. Mater.* **2002**, *14*, 2120–2128.
(2) Carrettin, S.; Corma, A.; Iglesias, M.; Sanchez, F. *Appl. Catal., A* **2005**, *291*, 247–252.
(3) Baidya, T.; Marimuthu, A.; Hegde, M. S.; Ravishankar, N.; Madras, G. *J. Phys. Chem. C* **2007**, *111*, 830–839.
(4) Singh, U. G.; Li, J.; Bennett, J. W.; Rappe, A. M.; Seshadri, R.; Scott, S. L. *J. Catal.* **2007**, *249*, 349–358.
(5) Li, J.; Singh, U. G.; Schladt, T. D.; Stalick, J. K.; Scott, S. L.; Seshadri, R. *Chem. Mater.* **2008**, *20*, 6567–6576.
(6) Baidya, T.; Dutta, G.; Hegde, M. S.; Waghmare, U. V. *J. Chem. Soc., Dalton Trans.* **2009**, 455–464.
(7) Hegde, M. S.; Madras, G.; Patil, K. C. *Acc. Chem. Res.* **2009**, *42*, 704–712.
(8) Haruta, M. *Catal. Today* **1997**, *36*, 153–166.
(9) Ishida, T.; Haruta, M. *Angew. Chem., Int. Ed.* **2007**, *46*, 7154–7156.
(10) Fierro-Gonzalez, J. C.; Guzman, J.; Gates, B. C. *Topics Catal.* **2007**, *44*, 103–114.
(11) Fu, Q.; Saltsburg, H.; Flytzani-Stephanopoulos, M. *Science* **2003**, *301*, 935–938.
(12) Kim, C. H.; Thompson, L. T. *J. Catal.* **2005**, *230*, 66–74.
(13) Guzman, J.; Gates, B. *J. Am. Chem. Soc.* **2004**, *126*, 2672–2673.
(14) Hutchings, G. J.; Hall, M. S.; Carley, A. F.; Landon, P.; Solsona, B. E.; Kiely, C. J.; Herzing, A.; Makkee, M.; Moulijn, J. A.; Overweg, A.; Fierro-Gonzalez, J. C.; Guzman, J.; Gates, B. C. *J. Catal.* **2006**, *242*, 71–81.
(15) Yang, J. H.; Henao, J. D.; Raphulu, M. C.; Wang, Y. M.; Caputo, T.; Groszek, A. J.; Kung, M. C.; Scurrell, M. S.; Miller, J. T.; Kung, H. H. *J. Phys. Chem. B* **2005**, *109*, 10319–10326.
(16) Schwartz, V.; Mullins, D.; Yan, W.; Chen, B.; Dai, S.; Overbury, S. *J. Phys. Chem. B* **2004**, *108*, 15782–15790.
(17) Weiher, N.; Bus, E.; Delannoy, L.; Louis, C.; Ramaker, D.; Miller, J.; van Bokhoven, J. *J. Catal.* **2006**, *240*, 100–107.
(18) Xu, C.; Xu, X.; Su, J.; Ding, Y. *J. Catal.* **2007**, *252*, 243–248.
(19) Zanella, R.; Giorgio, S.; Shin, C.; Henry, C.; Louis, C. *J. Catal.* **2004**, *222*, 357–367.
(20) Zhang, X.; Shi, H.; Xu, B. *Angew. Chem., Int. Ed.* **2005**, *44*, 7132–7135.
(21) Guan, Y.; Hensen, E. J. M. *Phys. Chem. Chem. Phys.* **2009**, *11*, 9578–9582.

Published on Web 04/15/2010

thought it of interest to prepare and carefully characterize two well-defined oxide compounds containing the ions Au^{3+} and Pd^{2+}, and given their similar electronic propensities (square-planar d^8), to compare their reactivities in the light of their electronic structures. We develop this theme in the following.

Au is a unique metal in that it does not form a well-defined binary compound with oxygen. Typical of a heavy metal however, Au does admit of soft interactions, and is naturally found in a bound state in the telluride mineral calaverite $AuTe_2$. The paucity of known oxoaurates is unsurprising given the oxophobic nature of gold, which is the most electronegative of metals. A few dozen mixed-metal oxides containing gold have, however, been prepared, and many of these are included in the review by Muller-Buschbaum.[22] To make oxygen reactive toward gold, it helps to create the necessary conditions for covalent oxygen−gold interactions. These would arise in a structure where oxygen is otherwise only weakly bound to the other cations. Such a concept has been applied to the stabilization of a variety of 3d transition metals in unusually high oxidation states. Mixed oxides containing Fe^{4+},[23,24] Fe^{5+},[25,26] Co^{4+},[27] Ni^{4+},[28,29] and Cu^{3+}[30] are stabilized through the covalent M−O interactions that arise when highly electropositive counter-cations are present to drive electron donation from O to the more electronegative transition metals, as discussed by Etourneau et al.[31] The majority of the known mixed metal oxides with gold therefore contain relatively large and electropositive alkali, alkaline earth, or rare earth ions as the other metal ion. Many of the known oxide compounds with gold cations require high pressure synthesis; only a few of the oxides presented in the literature can be prepared at atmospheric pressure in air, and of these, very few are stable under ambient conditions.

First reported by Abbattista et al.,[32] the compound $La_2Li_{1/2}Au_{1/2}O_4$ was originally believed to adopt the ordered K_2NiF_4 Ruddlesden−Popper (RP) structure, with slabs of corner-shared, octahedral Li^+ and Au^{3+}. Single crystal X-ray diffraction studies[33] revealed that the structure is actually based on a superstructure of Nd_2CuO_4, with square planar coordination around lithium and gold, and the two cations arranging themselves in a 2D rock-salt structure depicted in Figure 1.

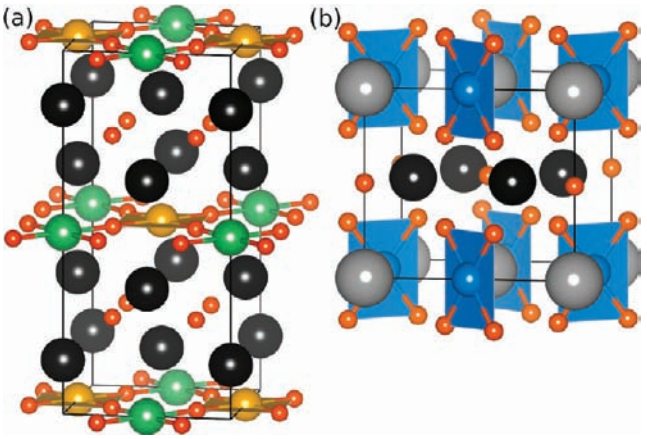

Figure 1. (a) Crystal structure of La_4LiAuO_8. Isolated square planes of AuO_4 are depicted. These are separated by LiO_4, which corner share with one-another in the plane. The planes are separated by layers of La and O. Green spheres are Li, gold spheres are Au, orange are O, and dark gray are La. (b) Crystal structure of La_2BaPdO_5. The isolated square planes of PdO_4 are depicted. Blue spheres are Pd, light gray spheres are Ba, orange are O, and dark gray are La.

La_4LiAuO_8 can alternately be described as possessing slabs of corner-connected squares of LiO_4 and AuO_4, separated by fluorite-type bilayers of La and O (Figure 1). A study of polycrystalline samples in the rare-earth series $Ln_2Li_{1/2}Au_{1/2}O_4$ (Ln = La, Nd, Sm, Eu, Gd) included a Mössbauer study of Au in $Nd_2Li_{1/2}Au_{1/2}O_4$ to definitively assign the oxidation state of gold as Au^{3+}.[34] In the same study, ^{7}Li NMR of the La compound was also performed, and indicated the presence of two Li environments, possibly arising from anti-site disorder between Li and Au in the sheets.[34] Rietveld refinements in the originally proposed, incorrect K_2NiF_4 structure were appreciably improved by modeling Au/Li site disorder.[32] Disorder was not included in the modeling in the single crystal study.[33] A first-principles study of the electronic structure was reported by Mattheiss,[35] where it was shown that metallic behavior is predicted for the K_2NiF_4-type structure (T-type) with octahedral coordination around Au and Li, while a band gap is present in the Nd_2CuO_4 (T'-type) structure where Au and Li are square planar. A band gap would be consistent with the reported yellow color of the material.

La_2BaPdO_5, reported originally by Taniguchi et al.,[36] is isostructural with Y_2BaPdO_5,[37] and contains isolated PdO_4 square planes (Figure 1). A series of closely related platinates, Ln_2BaPtO_5 (Ln = Nd, Eu, Sm, Gd), were considered for application in 3-way automotive emissions catalysis (oxidation of CO and hydrocarbons, and reduction of NO_x species);[38] however, the study was focused on the viability of using the mixed oxides as alternative materials rather than an examination of the reactivity of oxides compared to oxide-supported metal nanoparticles. Mechanisms proposed for the oxidation of CO by Pd^{2+} typically involve the participation of lattice oxide vacancies.[3] La_2BaPdO_5 offers a fully

(22) Muller-Buschbaum, H. *Z. Anorg. Allg. Chem.* **2002**, *628*, 2559–2584.
(23) Demazeau, G.; Chevreau, N.; Fournes, L.; Soubeyroux, J.; Takeda, Y.; Thomas, M.; Pouchard, M. *Rev. Chim. Miner.* **1983**, *20*, 155–172.
(24) Demazeau, G.; Pouchard, M.; Chevreau, N.; Colombet, J.; Thomas, M.; Menil, F.; Hagenmuller, P. *J. Less-Common Met.* **1980**, *76*, 279–283.
(25) Buffat, B.; Demazeau, G.; Pouchard, M.; Fournes, L.; Dance, J.; Fabritchnyi, P.; Hagenmuller, P. *C.R. Acad. Sci., Ser. IIb: Mec., Phys., Chim., Astron.* **1981**, *292*, 509–511.
(26) Demazeau, G.; Buffat, B.; Menil, F.; Fournes, L.; Pouchard, M.; Dance, J.; Fabritchnyi, P.; Hagenmuller, P. *Mater. Res. Bull.* **1981**, *16*, 1465–1472.
(27) Buffat, B.; Demzeau, G.; Pouchard, M.; Dance, J.; Hagenmuller, P. *J. Solid State Chem.* **1983**, *50*, 33–40.
(28) Lander, J. *Acta Crystallogr.* **1951**, *4*, 148–156.
(29) Takeda, Y.; Kanamaru, F.; Shimada, M.; Koizumi, M. *Acta Crystallogr., Sect. B: Struct. Sci.* **1976**, *32*, 2464–2466.
(30) Demazeau, G.; Parent, C.; Pouchard, M.; Hagenmuller, P. *Mater. Res. Bull.* **1972**, *7*, 913–920.
(31) Etourneau, J.; Portier, J.; Menil, F. *J. Alloys Compd.* **1992**, *188*, 1–7.
(32) Abbattista, F.; Vallino, M.; Mazza, D. *J. Less-Common Met.* **1985**, *110*, 391–396.
(33) Pietzuch, W.; Warda, S. A.; Massa, W.; Reinen, D. *Z. Anorg. Allg. Chem.* **2000**, *626*, 113–117.
(34) Tresse, F.; Demazeau, G.; Sanchez, J. P.; Fournes, L.; Suh, K. S. *J. Solid State Chem.* **1993**, *103*, 95–104.
(35) Mattheiss, L. F. *Phys. C* (*Amsterdam, Neth.*) **1995**, *251*, 140–148.
(36) Taniguchi, T.; Kawaji, Y.; Ozawa, T.; Nagata, Y.; Noro, Y.; Samata, H.; Lan, M. *J. Alloys Compd.* **2005**, *386*, 63–69.
(37) Laligant, Y.; Férey, G.; Hervieu, M.; Raveau, B. *Eur. J. Solid State Inorg. Chem.* **1988**, *25*, 111–117.
(38) Hietikko, M.; Suhonen, S.; Pursiainen, J.; Laitinen, R.; Valden, M.; Savimaki, A.; Slotte, T.; Harkonen *Appl. Catal., B* **2002**, *37*, 243–255.

stoichiometric compound, and should act as a good model for elucidating the activity of square planar Pd^{2+} ions in the solid state, with the activity being delineated from simply one of mobilizing the transport of oxide ions. The present study is the first report of a pure (rather than lightly substituted) Pd^{2+} oxide being used for the catalytic conversion of CO to CO_2.

Here we report the preparation and characterization of polycrystalline La_4LiAuO_8 and La_2BaPdO_5, oxides that contain isolated AuO_4 and PdO_4 square planes, respectively. We present them as model compounds for examining the role of (isoelectronic square planar) Au^{3+} and Pd^{2+} in heterogeneous catalysis. The structure, stability, surface characteristics, and electronic structure of these compounds are emphasized, investigated with techniques including synchrotron X-ray scattering, X-ray photoelectron spectroscopy, thermogravimetric analysis (TGA) under different gaseous atmospheres, and density functional calculations of the electronic structures. TGA suggests the compounds are remarkably stable toward thermal decomposition and even reduction. The activity of the two compounds as heterogeneous catalysts has been tested in the oxidation of CO to CO_2. La_2BaPdO_5 seems to effectively catalyze the conversion of CO to CO_2, while La_4LiAuO_8 is not at all effective at catalyzing this transformation. The differences in the reactivities of the two compounds are discussed with respect to differences in their density functional electronic structures.

Methods

La_4LiAuO_8 was prepared from stoichiometric mixtures of $La(OH)_3$ (Aldrich, 99.9%) and Au powder (Cerac, 99.95%), thoroughly ground with a 50% molar excess of $LiOH \cdot H_2O$ (Aldrich, $\geq$ 98%) in an agate mortar. Mixtures were pelletized and heated on silver foil in air or in flowing O_2 at 750 °C for 30 h with two intermittent grindings. The sample used in the synchrotron scattering studies was prepared entirely in air. Pale, yellow-gold powders were obtained. Evolution of the target phase was monitored between heating cycles (Phillips X′PERT MPD, CuK_α radiation). Samples treated in flowing O_2 did not have the gold tint of samples synthesized entirely in air, appearing a bright but still pale yellow. Excess lithium was removed from samples by washing in deionized water and drying at 150 °C. A fully reduced sample was prepared by heating La_4LiAuO_8 in flowing 5%-H_2 (N_2 balance) at 600 °C for 5 h. A larger 2 g batch prepared for ^{6}Li NMR showed a significant amount of La_2O_3 and *fcc*-Au metal after 30 h of heating, ≈10% La_2O_3 and 1% Au(0) by weight from quantitative Rietveld analysis of X-ray diffraction (XRD) data, and was treated for an additional 20 h (10 h × 2) in flowing O_2. The additional heating did not lead to entirely phase pure product, but did yield a sample of comparable purity to the smaller batches that were prepared, with La_2O_3 and Au^0 present in less than 4% by weight.

La_2BaPdO_5 was prepared using the method described by Taniguchi et al.[36] Stoichiometric mixtures of La_2O_3 (Alfa Aesar, 99.99%), $BaCO_3$ (Johnson and Matthey Specialty Products), and PdO (Cerac, 99.95%) were ground in an agate mortar and calcined in air for 10 h at 800 °C in a zirconia crucible. The mixture was reground and pelletized, and to avoid contact with the crucible the pellet was heated on a bed of powder of the component mixture ("containerless" reactions) at 900 °C in air for 10 h. The color of the sample changed from brown to beige after heating at 900 °C. After regrinding, the mixture was pressed into a pellet and heated containerless at 1100 °C for 10 h in flowing O_2. This was repeated three times to obtain phase-pure yellow La_2BaPdO_5. A reduced sample was prepared by heating La_2BaPdO_5 in flowing 5%-H_2 (N_2 balance) at 750 °C for 10 h.

Sample purity and the products of reduction were studied using XRD data acquired on a Philips X′PERT diffractometer with $CuK\alpha$; radiation. Thermogravimetic analysis (TGA) was performed on a Cahn TG-2141, monitored in different atmospheres between room temperature (RT) and 950 °C for La_4LiAuO_8, and between RT and 1000 °C (5% H_2) or 1100 °C (N_2 and air) for La_2BaPdO_5, with a ramp rate of 5 °C/min, and 2 h dwell time at the maximum temperature.

Synchrotron X-ray scattering data were collected at RT in transmission mode on beamline 11-ID-B at the Advanced Photon Source (Argonne National Laboratory) with an X-ray energy near 90 keV, with samples contained in Kapton tubes. The experimental setup has been described by Chupas et al.[39] Scattering data for La_4LiAuO_8 were collected with an image plate system (MAR345) at sample-to detector distances of ≈970 mm for Rietveld analysis, and ≈230 mm for pair distribution function (PDF) analysis. Scattering data for La_2BaPdO_5 were collected on an amorphous silicon detector plate (GE) at a sample-to-detector distance of ≈650 mm. The image plate data were processed using the program FIT2D.[40] A single exposure was collected for Rietveld analysis. Data for PDF analysis were collected using three exposures and averaged. The PDF, $G(r) = 4\pi r[\rho(r) - \rho_0]$,[41,42] was extracted with the program PDFGetX2,[43] using a maximum momentum transfer of $Q = 20$ Å^{-1}. Bulk cubic CeO_2 was used as a calibration standard, and yielded an effective wavelength of $\lambda = 0.1370$ Å, as well as instrument parameters for PDF analysis. The Rietveld method[44] was used to refine lab and synchrotron X-ray data as implemented by the XND Rietveld code[45] and synchrotron Rietveld data was also analyzed by MEM/Rietveld method with RIETAN-2000[46] and PRIMA[47] to map the charge density in La_4LiAuO_8 and La_2BaPdO_5. The unit cell depiction, charge density isosurfaces and slices were visualized using VESTA.[48] Full structure profile refinements with the PDF data were carried out in the program PDFFIT2 and PDFgui.[49] Bond valence analyses were carried out with the Bond Valence Caculator.[50] For Au^{3+}, the bond valence parameter determined by Brese and O'Keeffe was used.[51]

X-ray photoelectron spectra were obtained on a Kratos Axis Ultra spectrometer with a monochromatic Al $K\alpha$; source ($E = 1486$ eV). Samples were mounted on a stainless steel sample holder using double-sided carbon tabs. The residual pressure inside the analysis chamber was below 7.0×10^{-9} Torr. Survey spectra over a wide range of binding energies were acquired using an analyzer pass energy of 80 eV. Higher-resolution spectra of Au 4f and Pd 3d levels were collected at a pass energy of 20 eV, with binding energies measured to a precision of ±0.2 eV. Binding energy corrections

(39) Chupas, P.; Qiu, X.; Hanson, J.; Lee, P.; Grey, C.; Billinge, S. *J. Appl. Crystallogr.* **2003**, *36*, 1342–1347.
(40) Hammersley, A.; Svensson, S.; Hanfland, M.; Fitch, A.; Hausermann, D. *High Pressure Res.* **1996**, *14*, 235–248.
(41) Cullity, B.; Stock, S. *Elements of X-ray Diffraction*, 3rd ed.; Prentice Hall: Upper Saddle River, NJ, 2001.
(42) Egami, T.; Billinge, S. *Underneath The Bragg Peaks: Structural Analysis of Complex Materials*; Pergamon Press Elsevier: Oxford, England, 2003.
(43) Qiu, X.; Bozin, E.; Juhas, P.; Proffen, T.; Billinge, S. *J. Appl. Crystallogr.* **2004**, *37*, 110–116.
(44) Rietveld, H. *J. Appl. Crystallogr.* **1969**, *2*, 65.
(45) Bérar, J.-F.; Garnier, P. *NIST Spec. Publ.* **1992**, *846*, 212.
(46) Izumi, F.; Ikeda, T. *Mater. Sci. Forum* **2000**, *321−324*, 198–203.
(47) Izumi, F.; Dilanian, R. A. *Transworld Res. Network* **2002**, *3*, 699–726.
(48) Momma, K.; Izumi, F. *J. Appl. Crystallogr.* **2008**, *41*, 653–658.
(49) Farrow, C. L.; Juhas, P.; Liu, J. W.; Bryndin, D.; Bozin, E. S.; Bloch, J.; Proffen, T.; Billinge, S. J. L. *J. Phys.: Condens. Matter* **2007**, *19*, 335219.
(50) Hormillosa, C.; Healy, S.; Stephen, T.; Brown, I. D. *Bond Valence Calculator*, Version 2.0; 1993; http://ccp14.ac.uk.
(51) Brese, N. E.; O'Keeffe, M. *Acta Crystallogr.* **1991**, *B47*, 192–197.

from sample charging effects were made by calibrating to the C 1s electron peak at 285.0 eV. Mixed Gaussian−Lorentzian functions were used to model the Au-$4f_{7/2}$/Au-$4f_{5/2}$ and Pd-$3d_{5/2}$/Pd-$3d_{3/2}$ doublets, constrained to an integrated area ratio of 0.75 (0.67), and to a peak separation of 3.67 eV (5.26 eV).

^{6}Li NMR experiments were carried out on a Bruker AVANCE 500 MHz WB spectrometer, operating at 73.6 MHz for ^{6}Li, with a Bruker 4 mm double resonance H/X MAS probe. Typical parameters used in the single pulse method are as follows: pulse length 3 μs (45°), acquisition time 20.5 ms, spectral width 68 ppm, relaxation delay 5 s, magic angle spinning frequency 10 kHz, and the total number of scans were 28000 and 34000 for samples before and after washing, respectively. The chemical shift was referenced to a 1 M solution of LiCl.

Diffuse reflectance UV/vis spectra were recorded in the wavelength range 220 to 800 nm using a Shimadzu UV-3600 spectrometer equipped with an ISR-3100 integrating sphere. Samples were mixed with $BaSO_4$. The absorbance spectrum was obtained by applying the Kubelka−Munk relation $F(R) = (1 - R^2)(2R)^{-1}$.[52,53]

The surface areas of reduced La_4LiAuO_8 and reduced La_2BaPdO_5 were measured on a Micromeritics TriStar 3000 BET Analyzer. N_2 was used as the analysis gas, and liquid N_2 was used as the cryogen. Powder samples were dried and degassed by heating at 250 °C for 3 h under flowing N_2 before measurement. The free space in the sample tubes were determined with He, which was assumed to not adsorb. The surface areas of as-prepared La_4LiAuO_8 and La_2BaPdO_5 could not be determined accurately by N_2 sorption because they are below the detection limit of the BET method, but can be estimated as $\approx$1 m^2 g^{-1}.

Catalytic experiments were carried out in a Hiden CATLAB fixed-bed tubular quartz microreactor of dimensions 18 cm ×0.4 cm (inner diameter), located in a tubular oven with temperature control between RT and 1100 °C. Catalyst samples (25 mg, 60 mesh) were diluted with cordierite (100 mg, 40/80 mesh, NGK Honeyceram), loaded in the reactor to give a bed length about 1 cm, and held in place at each end with quartz wool. The reactor was operated at a total pressure of 1.0 atm, and the pressure drop (< 0.03 atm) was neglected. The reaction temperature was monitored by a K-type thermocouple touching the catalyst bed. Reactant and product compositions were monitored by an online quadrupole mass spectrometer (HR-20, Hiden Analytical Ltd., U.K.). The oxidation of CO was studied as a temperature-programmed reaction, using premixed 1000 ppm CO/9.5% O_2/Ar balance (AccuAir), and a flow rate of 50 cm^3 min^{-1}. Conversion was monitored using the signal at m/e = 44 for CO_2, after baseline correction with the feed gas (no catalyst) and calibration using a standard gas mixture containing 1000 ppm CO_2.

Density functional electronic band structures were calculated using the linear muffin-tin orbital (LMTO) method[54,55] performed within the atomic sphere approximation. Scalar-relativistic Kohn−Sham equations were solved within the local-density approximation.[56] In addition, all relativistic effects were taken into account except for the spin−orbit coupling. For La_4LiAuO_8, the calculations were performed on 441 irreducible k points within the primitive wedge of the Brillouin zone, while the calculations on La_2BaPdO_5 employed 360 irreducible k points. The input crystal structures for the calculations were obtained from the reported single crystal structure of La_4LiAuO_8,[33] and from the synchrotron diffraction study reported here for La_2BaPdO_5. Crystal orbital Hamiltonian populations (COHP) were calculated following the prescription of Dronskowski and Blochl[57] as a means of extracting the strength of Au−O and Pd−O interactions from the electronic structure calculations.

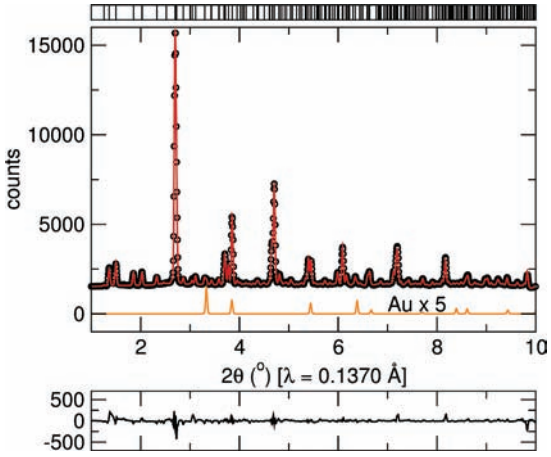

Figure 2. Rietveld refinement of synchrotron powder diffraction pattern collected with a X-ray energy near 90 keV. The open circles are data, red line is the Rietveld fit, the contribution from *fcc*-Au metal is shown, multiplied by 5, below the fit, and the trace at the bottom is the difference profile. Vertical lines at the top of the figure are the expected peak positions for La_4LiAuO_8. Peak positions for La_2O_3, $La(OH)_3$, and Au not shown.

Results and Discussion

La_4LiAuO_8. Preparation and Structure. Nearly phase-pure yellow La_4LiAuO_8 samples were obtained when a 50% molar excess of $LiOH \cdot H_2O$ was used, and following three cycles of heating at 750 °C for 10 h with intermediate grinding, with the samples contained in silver foil. No apparent corrosion of the silver foil was noted after the reaction. The reactions were performed both in air and in flowing O_2, and there is some evidence from X-ray diffraction and X-ray photoelectron spectroscopy (XPS) that heating in O_2 results in slightly cleaner final product distributions. However, in neither case were the samples completely phase pure.

The results of synchrotron X-ray Rietveld analysis performed on a sample prepared in air are displayed in Figure 2. The use of a very short wavelength, λ = 0.1370 Å, ensures a large scattering range and stable refinements of all parameters. The impurities in the final product were identified as La_2O_3, $La(OH)_3$, and *fcc*-Au, and quantitative phase analysis estimated all of these to be less than 4 wt % with respect to the main phase. Crystal structure parameters obtained from the Rietveld refinement are compared in Table 1 with values reported from the single crystal structure determination of Pietzuch et al.[33]

It was necessary to introduce Li/Au anti-site disorder in the Rietveld model to obtain a satisfactory fit, refining the extent of site exchange, δ as defined by writing the formula of the compound $La_4Li_{1-\delta}Au_\delta Au_{1-\delta}Li_\delta O_8$. At the end of the refinement, δ was found to have the value 0.082(2), suggesting that approximately 8% of the Li sites have Au atoms on them and vice versa. The position of O1

(52) Kubelka, P.; Munk, F. *Z. Tech. Phys.* **1931**, *12*, 593–601.
(53) Kubelka, P. *J. Opt. Soc. Am.* **1948**, *38*, 448–457.
(54) Andersen, O. K. *Phys. Rev. B* **1975**, *12*, 3060–3083.
(55) Jepsen, O.; Andersen, O. K. *Z. Phys. B* **1994**, *97*, 35–47.
(56) von Barth, U.; Hedin, L. *J. Phys. C: Solid State Phys.* **1972**, *5*, 1629–1642.
(57) Dronskowski, R.; Bloechl, P. E. *J. Phys. Chem.* **1993**, *97*, 8617–8624.

Table 1. La_4LiAuO_8[a]

	Rietveld	PDF	single crystal
a (Å)	5.757(1)	5.742(2)	5.768(<1)
b (Å)	5.762(1)	5.758(2)	5.762(<1)
c (Å)	12.465(1)	12.446(2)	12.466(1)
V (Å^3)	413.5(1)	411.5(2)	414.28(7)
La1, z	0.1489(1)	0.1495(4)	0.14907(3)
La1, U_{eq}	0.0062(3)	0.0050(2)	0.0023(1)
La2, z	0.3499(1)	0.3503(4)	0.35036(3)
La2, U_{eq}	0.0062(3)	0.0050(2)	0.0022(1)
Li/Au, δ	0.082(2)	0	0
Li/Au, U_{eq}	0.010(1)	0.0049(4)	0.0025(1)
O1, x	0.259(2)	0.261(6)	0.2530(5)
O1, y	0.253(2)	0.256(6)	0.2469(6)
O1, U_{eq}	0.012(3)	0.021(4)	0.0071(9)
O2, x	0.265(2)	0.234(6)	0.2492(5)
O2, U_{eq}	0.004(2)	0.018(3)	0.0051(8)

[a] Space group *Ammm* (No. 65). The atom positions are: La1 (4*i*) at (0,0,z), La2 (4*j*) at (1/2,0,z), Li (2*b*) at (0,0,1/2), Au (2d) at (1/2,0,0), O1 (8*o*) at (x,y,0) and O2 (8*m*) at (x,1/4,1/4). δ refers to the extent of mixing between Li and Au, when the composition is written $La_4Li_{1-\delta}Au_\delta$-$Au_{1-\delta}Li_\delta O_8$. The single crystal results are taken from reference 33.

Table 2. Bond Valence Sums Calculated from the Cation-Anion Distances Obtained from the Different Structural Analyses

	Rietveld	PDF	single crystal
Au	2.9	2.9	2.9
Li	0.8	0.9	0.8
La1	2.7	3.5	3.0
La2	3.4	3.0	3.0
O1	1.7	1.8	2.0
O2	2.2	2.4	2.0

was strongly correlated with δ. Au−O and Li−O bond distances were significantly affected by the modeling of site exchange, but agreed well with the published ordered structure once the model was relaxed. To obtain a stable refinement of the occupancy, the total amounts of Li and Au in the unit cell were set to unity, and the thermal parameters of Li and Au were constrained to the same refined value. The thermal parameters for La1 and La2 were similarly constrained. The introduction of site exchange notably improved refinement statistics, which converged at $R_{wp} = 4.3\%$ and $\chi^2 = 1.14$. It is interesting that the single crystal study of Pietzuch et al.[33] is reported to have been performed on a fully ordered crystal with $\delta = 0$.

Bond valence sums (BVS) extracted for all ions from the near-neighbor distances obtained in the Rietveld refinement are displayed in table Table 2. The BVS values calculated from the single crystal structural data presented by Pietzuch et al.[33] almost precisely match the expected valences, with the exception of Au and Li which are both slightly underbonded. The discrepancies between expected bond valence sums for the different ions and the values obtained from Rietveld analysis are a little larger.

The structure obtained from Rietveld analysis was used as a starting model in the analysis of the PDF. However, all PDF refinements converged, within experimental error, to values of the site mixing $\delta = 0$, implying that the local structure is best described by an absence of Li/Au anti-site disorder. With regards to disorder, the local structure as obtained from the PDF analysis is therefore distinct from the average structure obtained from Rietveld refinement which does suggest anti-site disorder

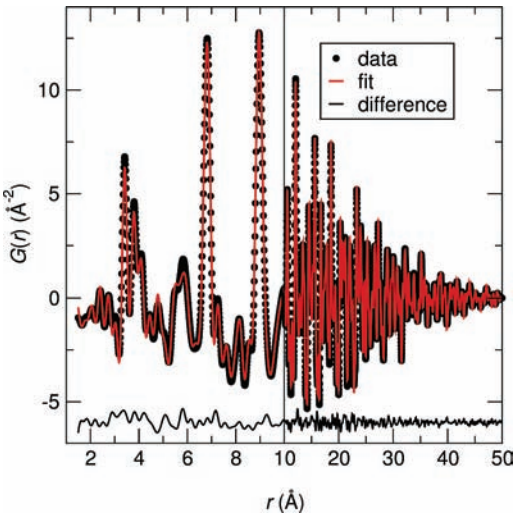

Figure 3. PDF refinement of synchrotron powder diffraction pattern collected with an X-ray energy of 90 keV. The circles are data, the red line is the fit to the bulk crystal crystal structure without anti-site disorder, and the trace at the bottom is the difference profile.

(Figure 3). Structural parameters obtained from the refinement of the PDF to 50 Å are presented in Table 1, with BVS extracted from all the near-neighbor distances presented in Table 2. The PDF analysis yields cation−anion distances which are very similar to those obtained from the Rietveld analysis. Lattice parameters obtained from synchrotron PDF refinements typically show some differences with those calculated in Rieveld refinements, owing to the effects of instrumental broadening in the scattering data that are not removed before generation of the PDF.[43]

The Maximum entropy method (MEM/Rietveld) was employed to determine the charge density distribution in La_4LiAuO_8. The MEM offers many advantages in extending the useful information obtainable from diffraction data, independent of a structural model. MEM yields the most probable distribution of the numerical quantities over the ensemble of voxels.[58−60] Because of the difficulty in obtaining a satisfactory Rietveld refinement with an ordered structure, only the disordered model was considered in the MEM study. The 268 observed structure factors derived from the Rietveld analysis and estimates of the structure factors for 16 additional reflections were used in the MEM analysis. The analysis was performed with the unit cell divided into 64 × 64 × 128 voxels. The weighted R factor based on the structure factors for the final MEM charge density is 3.9%.

Equicontour isosurfaces are shown in Figure 4(a), and a projection of the electron density on the (110) plane of the structure in Figure 4(b). No residual density was observed apical to lithium, even though Li is commonly sited in the centers of distorted octahedra in Ruddlesden−Popper type perovskites. The electron density between Au and O is indicative of the covalent character in the Au−O bonding, and this is distinctly not seen in the region between Li and O. We return to this aspect of

(58) Collins, D. M. *Nature* **1982**, *298*, 49.
(59) Takata, M.; Nishibori, E.; Sakata, M. *Z. Kristallogr.* **2001**, *216*, 71.
(60) Nishimura, S.-I.; Kobayashi, G.; Ohoyama, K.; Kanno, R.; Yashima, M.; Yamada, A. *Nat. Mater.* **2008**, *7*, 707.

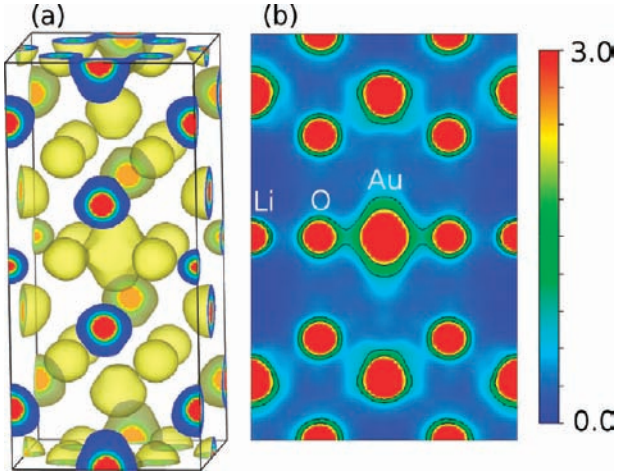

Figure 4. (a) MEM electron density displayed within the unit cell of La_4LiAuO_8. The isosurface of the electron density is set to a value of 0.8 $Å^{-3}$. (b) Map of the electron density projected on the (110) planes. Some contour lines are drawn for clarity, shown on a linear scale, and color coded according to the bar on the right, ranging from 0.0 $Å^{-3}$ to 3.0 $Å^{-3}$ at intervals of 0.8 $Å^{-3}$. Note smearing in the electron density between Au and O suggestive of covalent bonding.

La_4LiAuO_8 in the text that follows, and point to the role that such covalency plays in stabilizing Au^{3+} in an oxide environment.

La_4LiAuO_8 was the subject of a ^7Li NMR study by Tresse et al.,[34] who observed two peaks separated by 3.5 ppm that they assigned to two different Li environments. We performed ^6Li studies, as this nucleus has a much smaller quadrupole moment, and compensated for its lower abundance by use of a relatively high-field instrument and collection of a large number of transients (>25000). The as-prepared La_4LiAuO_8 sample showed four signals in the ^6Li MAS NMR spectrum: two narrow resonances at −3.70 ppm and 0.27 ppm that integrated to relative populations of 69.5% and 11% respectively, and two broad peaks at 0.55 ppm and 2.9 ppm that integrated to relative populations of 10.5% and 9%. However, washing the sample in DI water led to the disappearance of both broad resonances, and a dramatic decrease in the intensity of the sharp signal at 0.27 ppm, Figure 5. We recall here that the samples are prepared with excess $LiOH \cdot H_2O$. The title compound therefore possesses a single Li environment with a resonance at −3.70 ppm.

From the XRD study, we expect that nearly 10% of the Li are involved in some sort of anti-site disordering with Au. This suggests that some of the Li might possess distinct chemical environments from others. It is clear, however, that if the additional NMR resonances were due to a distinct anti-site Li environment, the ratio of peak areas would not be affected by washing the excess LiOH used in preparation away from the sample. A single, isotropic, ^6Li signal suggests that the lithium environment is unaffected by the disorder in the average structure. The defects in La_4LiAuO_8 thus manifest in spite of the presence of coherent LiO_4/AuO_4 planes. This is also the finding from the PDF studies, and it is expected that the PDF is strongly weighted by the structural correlations within the LiO_4/AuO_4 planes, and is less strongly weighted by correlations between the planes, since these occur at longer vectors where there are contributions to

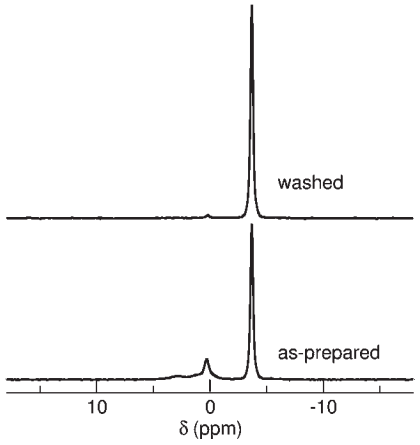

Figure 5. ^6Li MAS NMR of La_4LiAuO_8 before washing (bottom) and after washing with water (top). The suppression of all minor resonances after washing supports the presence of only one, isotropic, Li site.

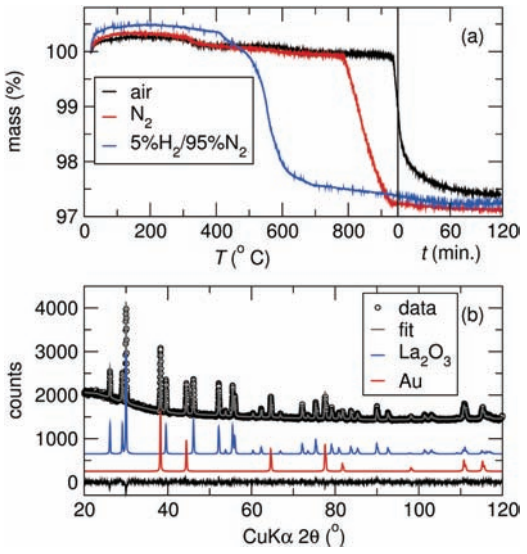

Figure 6. (a) TGA of La_4LiAuO_8 under different atmospheres. The approximate decomposition onset temperatures are 935 °C in air, 785 °C in N_2, and 480 °C in 5% H_2/Ar. (b) X-ray Rietveld analysis of the products of reduction showing complete conversion of La_4LiAuO_8 to La_2O_3 and *fcc*-Au, following TGA in N_2.

the $G(r)$ from many more atom−atom pairs. All evidence of anti-site disorder ($\delta \neq 0$) in the Rietveld analysis and in the MEM electron density, both of which are average techniques, are therefore suggested here as arising from faults in registry between different LiO_4/AuO_4 planes.

TGA. Considering the oxophobicity of gold, La_4LiAuO_8 is remarkably stable. The thermal stability of La_4LiAuO_8 in air, N_2, and 5%-H_2/Ar was monitored by TGA. The onset of rapid weight loss was observed at 935 °C in air, 785 °C in N_2, and 480 °C in the reducing atmosphere of 5%-H_2, as seen in Figure 6. Abbatista et al. reported a decomposition temperature of 890 °C in air, and identified the phase $LaLiO_2$ in products quenched from 900 °C.[32] The weight loss of 2.7% observed here corresponds to the formation of metallic Au and either, $2La_2O_3 + {}^1/_2Li_2O$, or $1.5La_2O_3 + LiLaO_2$. The smooth nature of the weight change suggests that there are no intermediates formed before complete reduction to *fcc* Au. We observed only one small diffraction peak that

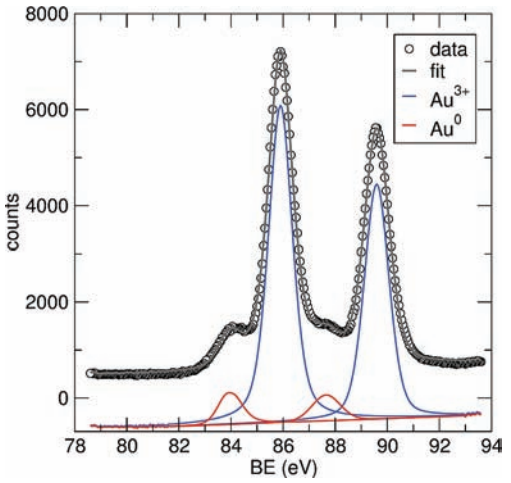

Figure 7. Au 4f XPS spectra of as-prepared La_4LiAuO_8. Observed Au $4f_{7/2}$ binding energies: Au^{3+} = 86.4 ± 0.2 eV, Au^0, bulk = 83.8 ± 0.2 eV.

could be indexed to $LiLaO_2$. The XRD of the sample decomposed in air showed mostly La_2O_3 and *fcc*-Au metal, though a small amount of La_4LiAuO_8 remained. Lanthanum hydroxide was also observed in some of the TGA products and in the sample reduced in 5%-H_2/N_2 for catalysis studies. Samples appeared dark brown immediately after decomposition, lightening to a maroon over time, possibly because of sintering of the initially formed small gold particles.

X-ray Photoelectron Spectroscopy. The Au 4f XPS spectrum for as-prepared La_4LiAuO_8 is shown in Figure 7. The spectrum reveals the presence of both Au^{3+} and Au^0 species. The observed Au^{3+} $4f_{7/2}$ binding energy of 86.4 ± 0.2 eV in La_4LiAuO_8 is slightly larger than reported for Au_2O_3 and $Au(OH)_3$, 85.9 eV.[61,62] Peaks corresponding to Au^0 were notably broader than the sharp peaks observed for bulk gold. Such line broadening has been observed for nanoparticulate gold.[63] A peak shift to higher binding energy occurs with a decrease in particle size, accompanied by substantial peak asymmetry on the higher energy side of the Au 4f peaks.[63,64] For example, Ono and Cuenya reported shifts of 0.3 ± 0.1 eV and 0.9 ± 0.1 eV to binding energies relative to bulk gold for 5 and 1.5 nm Au particles, respectively, supported on SiO_2.[64] The second gold phase corresponding to the Au^0 species may be a decomposition product of La_4LiAuO_8 rather than unreacted starting material. The ratio of integrated areas for Au^{3+} and Au^0 in the 4f region quantifies the amount of Au^0 on the grain surfaces to be 10 wt %. This is larger than that calculated from the scale factors of the multiphase Rietveld fits, and again suggests that some La_4LiAuO_8 decomposes on the surface. An alternate explanation is that the Au particles are not homogeneously distributed, and accumulate at or close to the surface of the powders. XPS of reduced samples showed a single contribution from metallic Au (84.0 eV). No evidence for Au^{1+} is found either in the as-prepared samples or the ones studied after reduction.

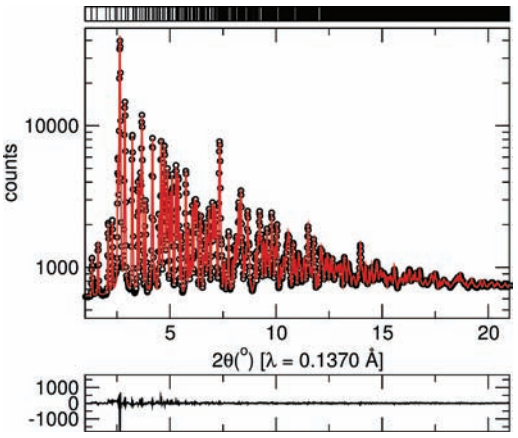

Figure 8. Rietveld refinement of synchrotron powder diffraction pattern collected with an X-ray energy near 90 keV. The open circles are data, red line is the Rietveld fit, and trace at the bottom is the difference profile. Vertical lines at the top of the figure indicate the expected peak positions.

Table 3. La_2BaPdO_5[a]

atom	*x*	*y*	*z*	U_{eq}	BVS
La	0.17324(6)	*x*+1/2	1/2	0.0035(1)	3.2
Ba	0	0	0	0.0081(2)	1.7
Pd	0	1/2	0	0.0036(2)	1.6
O1	0.3606(4)	*x*+1/2	0.2463(7)	0.006(1)	1.9
O2	0	0	1/2	0.003(2)	1.9

[a] Space group *P*4/*mbm* (No. 127). a = 6.8857(2) Å, c = 5.9274(3) Å, and V = 281.04(2) Å^3.

La_2BaPdO_5. Preparation and Structure. Phase-pure La_2BaPdO_5 was prepared from stoichiometric mixtures of La_2O_3, $BaCO_3$, and PdO, in the method described by Taniguchi et al.,[36] with calcination at 800 and 900 °C in air, followed by repeated heating in O_2 at 1100 °C with intermittent grindings. The color of the mixture changed from brown to beige after calcination at 900 °C. After each successive heating in O_2 the color of the powder became increasingly yellow. XRD confirmed the presence of small amounts of La_2O_3 and $BaCO_3$ remaining until after the fourth heating, after which an X-ray pure product was obtained. La_2BaPdO_5 is isostructural to Y_2BaPdO_5,[37] with isolated PdO_4 square planes, bicapped LaO_8 prisms, and bicapped BaO_{10} cubes.

The single-phase synchrotron X-ray Rietveld refinement for La_2BaPdO_5 is displayed in Figure 8, with crystal structure parameters obtained from the refinement given in Table 3. The amorphous silicon detector used to collect scattering data from La_2BaPdO_5 is larger than the MAR image plate used with La_4LiAuO_8 and provides a substantially wider angular range of data ($2\theta_{max}$ = 22°). Lattice parameters, atomic positions, and thermal parameters refined very stably, converging with a weighted R factor of 3.0% and χ^2 = 1.07. BVS extracted from near-neighbor distances indicate slight underbonding to Pd and Ba, with La slightly overbonded. This is consistent with valence sums calculated for the structures reported for Ln_2BaPdO_5 (*Ln* = Eu, Gd, Dy, Ho), which were determined by single crystal X-ray diffraction (Pd: 1.6 to 1.7; Ba: 1.8 to 1.9; *Ln*: 2.9 to 3.1).[65] The large relative

(61) Pireaux, J.; Liehr, M.; Thiry, P.; Delrue, J.; Caudano, R. *Surf. Sci.* **1984**, *141*, 221–232.
(62) Juodkazis, K.; Juodkazytè, J.; Jasulaitienè, V.; Lukinskas, A.; Šebeka, B. *Electrochem. Commun.* **2000**, *2*, 503–507.
(63) Zhang, P.; Sham, T. *Phys. Rev. Lett.* **2003**, *90*, 245502(1).
(64) Ono, L. K.; Cuenya, B. R. *J. Phys. Chem. C* **2008**, *112*, 4676–4686.
(65) Muller-Buschbaum, H.; Wulff, L. *Z. Naturforsch. B* **1996**, *51*, 461–464.

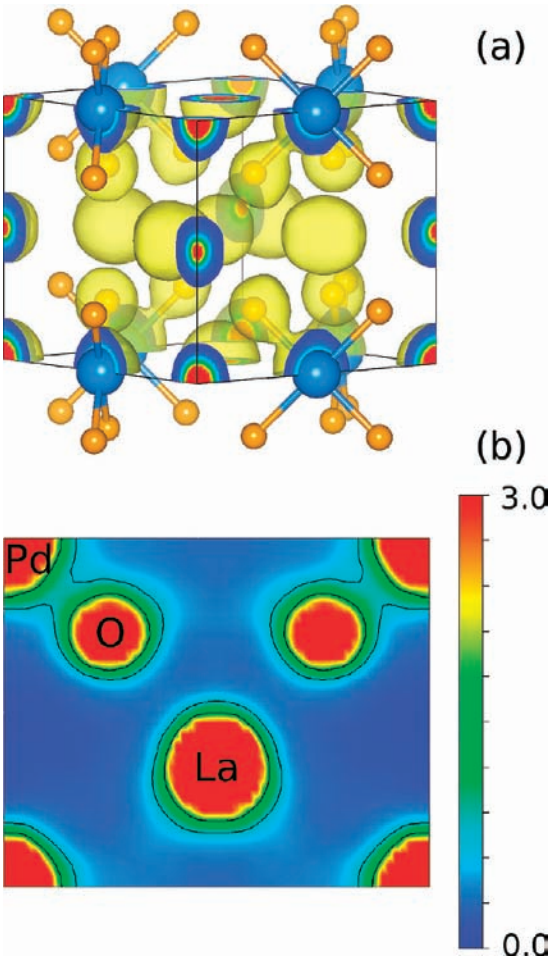

Figure 9. (a) MEM electron density displayed within the unit cell of La_2BaPdO_5. The isosurface of the electron density is set to a value of 0.8 Å $^{-3}$. Pd and O atoms are shown for clarity. (b) Map of the electron density projected on the (220) planes. Some contour lines are drawn for clarity, shown on a linear scale, and color coded according to the bar on the right, ranging from 0.0 Å $^{-3}$ to 3.0 Å $^{-3}$ at intervals of 0.8 Å $^{-3}$. Note smearing in the electron density between Pd and O suggestive of covalent bonding.

uncertainty in the thermal displacement factor for O2 reflects the difficulty in detecting oxygen with X-rays when present among heavy atoms.

MEM/Rietveld was also employed to determine the charge density distribution in La_2BaPdO_5. Structure factors derived from 1719 observed reflections in the Rietveld analysis and estimates for 86 additional structure factors were used in the MEM analysis, with the unit cell divided into 64 × 64 × 64 voxels. The weighted *R* factor for the final MEM charge density is 2.6%. Equicontour isosurfaces and a map of the charge density in the (220) plane are shown in Figure 9, panels a and b, respectively. The electron density between Pd and O indicates covalent character in the Pd−O bond. The covalency is caused by charge donation to oxygen by the highly electropositive La and Ba cations. As with La_4LiAuO_8, the localized bonding observed in La_2BaPdO_5 appears to be an important factor contributing to the stabilization of Pd^{2+} in an oxide environment.

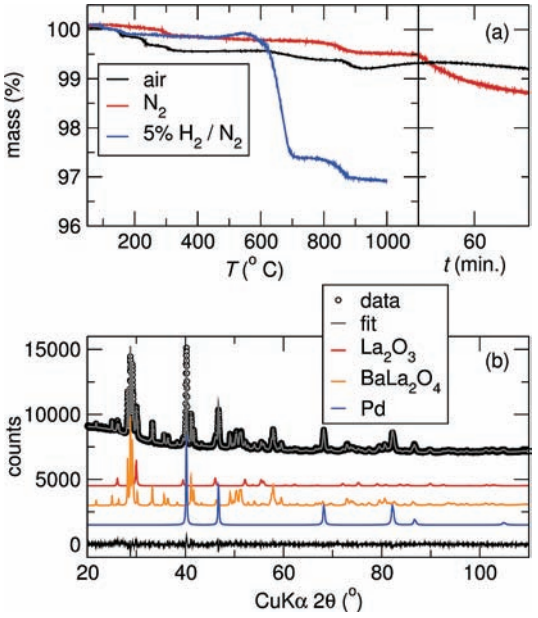

Figure 10. (a) TGA of La_2BaPdO_5 under air, insert, and reducing atmospheres. The approximate decomposition onset temperatures are 1090 °C in N_2, and 570 °C in 5% H_2/N_2. (b) X-ray Rietveld analysis of the products of reduction showing conversion of La_2BaPdO_5 to $BaLa_2O_4$, La_2O_3, and *fcc* Pd, following heat treatment in 5% H_2/Ar for 5 h at 700 °C.

TGA. The Pd^{2+} oxidation state is very effectively stabilized in La_2BaPdO_5. Whereas PdO decomposes in air at about 800 °C,[66] La_2BaPdO_5 is stable to almost 1100 °C in an inert atmosphere (N_2) and decomposes rather slowly at this temperature, as shown by TGA in Figure 10. The stability of La_2BaPdO_5 toward reduction in 5% H_2 is more remarkable, with the onset of decomposition not occurring until about 570 °C. For comparison, oxide-supported PdO is reduced below 100 °C under these conditions.[67] The localized Pd−O bonding observed in the MEM electron density determination is believed to impart the unusual thermal stability and resistance to reduction displayed by this compound.

A mass loss of 2.7 wt % corresponds to loss of one oxygen per formula unit in connection with the reduction of Pd^{2+}. The products identified by XRD in freshly reduced samples are Pd-metal, $BaLa_2O_4$, and La_2O_3 (Figure 10). The formation of La_2O_3, present at approximately 10 mol % by quantitative analysis of the powder diffraction pattern, is likely due to decomposition of $BaLa_2O_4$. The structure of $BaLa_2O_4$ for Rietveld refinement was adopted from $BaHo_2O_4$,[68] with starting lattice parameters taken from Mitamura et al.[69] Lattice parameters obtained in the refinement agree well with reported values. After 4 months of storage, no $BaLa_2O_4$ was observed by XRD, although it has been reported that this compound is quite sensitive to moisture.[69]

X-ray Photoelectron Spectroscopy. The Pd 3d XPS spectrum of as-prepared La_2BaPdO_5 is shown in Figure 11. The observed Pd-$3d_{5/2}$ binding energy of 337.4 eV is characteristic of Pd^{2+}, and is shifted to higher binding

(66) Zhang, H.; Gromek, J.; Fernando, G.; Boorse, S.; Marcus, H. *J. Phase Equilib.* **2002**, *23*, 246–248.

(67) Luo, M.; Zheng, X. *Appl. Catal., A* **1999**, *189*, 15–21.

(68) Doi, Y.; Nakamori, W.; Hinatsu, Y. *J. Phys.: Condens. Matter* **2006**, *18*, 333–344.

(69) Mitamura, T.; Ogino, H.; Kobayashi, H.; Mori, T.; Yamamura, H. *J. Am. Ceram. Soc.* **1993**, *76*, 2127–2128.

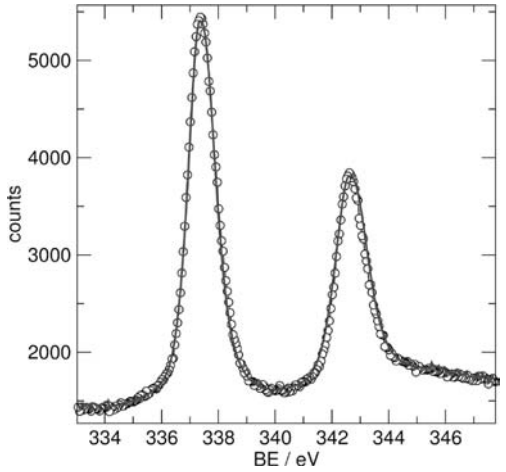

Figure 11. Pd 3d XPS spectra of as-prepared La_2BaPdO_5. Observed Pd $3d_{5/2}$ binding energy, $Pd^{2+} = 337.4 \pm 0.2$ eV.

energy than Pd^{2+} measured from a sample of PdO (336.8 eV), consistent with Pd in La_2BaPdO_5 being more ionic.[6,70] No contribution from metallic Pd is detected. Quantification of the cation ratios in the survey scan correspond well with the nominal stoichiometry, indicating a slightly Ba-rich surface composition: Pd (19.2%), Ba (22.3%), La (58.5%).

The XPS spectrum in the Pd 3d region of reduced La_2BaPdO_5 (not shown) contains contributions from two Pd states, a signal from Pd^0 at 334.8 eV, and a signal from an oxidized Pd species ($Pd^{\delta+}$) at 335.8 eV. The $Pd^{\delta+}$ contribution remained present even after reduction in 5% H_2 at 1000 °C, indicating a highly stabilized state, and the observed binding energy agrees with that reported in ref 71.

Electronic Structure and Optical Properties. Total densities of states (DOS), partial DOS of the Au 5d and Pd 4d states, and Au−O and Pd−O crystal orbital Hamiltonian populations from LMTO calculations are shown in panels (a), (b), and (c) of Figure 12, respectively, with the Fermi energy (E_F) referenced to the top of the valence band. The calculated band gap within the local density approximation is just a little smaller than 2 eV for La_4LiAuO_8, and about 2.4 eV for La_2BaPdO_5.

In La_4LiAuO_8, the Au 5d states form bonding combinations with the 2p states of O1, which neighbors Au, in the region centered at −5.5 eV. The filled Au d states extend to around −3.5 eV. Between −3 eV and the valence band maximum, states are largely derived from O1 and O2 2p (projections not shown). The empty states above the Fermi energy are once again Au 5d and, in a crystal field picture, would correspond to empty $d_{x^2-y^2}$ orbitals. These states are antibonding with O 2p orbitals. Characteristic of the interaction of filled d levels with filled p levels, there are also antibonding states just at the top of the valence band. The electronic structure is effectively that of a 16-electron square planar complex.

The electronic structure of La_4LiAuO_8 shares many similarities with isoelectronic La_2BaPdO_5; the Pd model

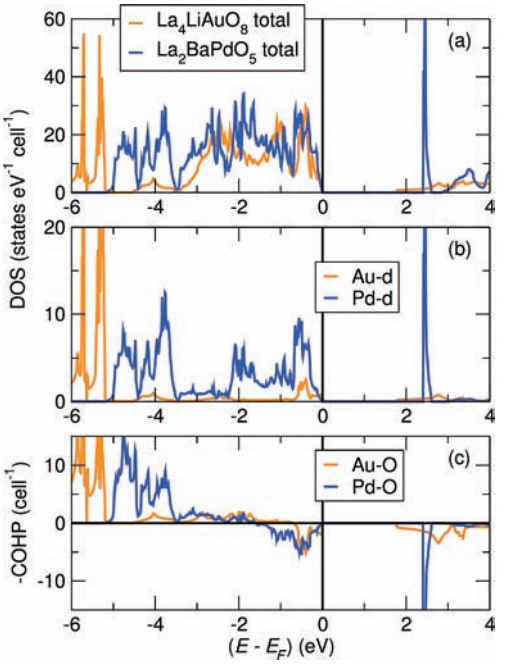

Figure 12. (a) LMTO-ASA densities of state for La_4LiAuO_8 and La_2BaPdO_5, including projected Au and Pd d states. (b) Crystal orbital Hamiltonian population (COHP) for a single $AuO(1)_4$ square, and a single $PdO(1)_4$ square. Most of the Au bonding states are centered at −5.5 eV in La_4LiAuO_8, with antibonding states just below and above the E_F. The bonding states in La_2BaPdO_5 are somewhat more dispersed and not found so deeply below E_F. The sharp antibonding feature at the conduction band edge reflects the pseudomolecular nature of the PdO_4 squares.

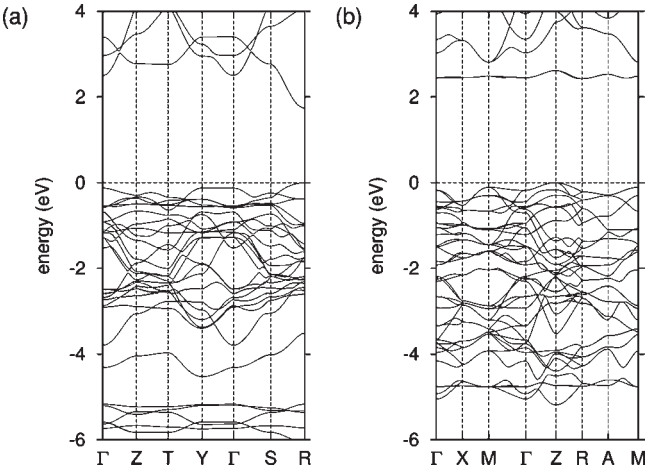

Figure 13. Energy band structures of (a) La_4LiAuO_8 and (b) La_2BaPdO_5.

compound can also be considered essentially a 16-electron square planar compound. In La_2BaPdO_5, however, the filled d states are more disperse and not as low in energy, and the empty d states are closer to the valence band maximum. The significantly lower filled d states of Au^{3+} in contrast to those in Pd^{2+} can be attributed in part to the higher positive charge on the cation, and the relativistic effects that make Au the most electronegative metal.

The band structure of La_4LiAuO_8 is displayed in panel (a) of Figure 13. The band gap arises from a direct transition at the R point of the Brillouin zone. The bands

(70) Li, J.; Singh, U. G.; Bennett, J. W.; Page, K.; Weaver, J.; Zhang, J. P.; Proffen, T.; Rappe, A. M.; Scott, S. L.; Seshadri, R. *Chem. Mater.* **2007**, *19*, 1418–1426.
(71) Tsyrul'nikov, P. G.; Afonasenko, T. N.; Koshcheev, S. V.; Boronin, A. I. *Kinet. Catal.* **2007**, *48*, 728–734.

with low dispersion centered at −5.5 eV have mostly Au 5d character, verified by constructing "fatbands"[55] (not shown here) which are a means of decorating the different energy bands with widths indicative of specific orbital contributions. The use of this technique also confirms that the band centered at −4 eV has some Au 5d character, as do bands just at the top of the valence band and at the bottom of the conduction band.

Figure 13(b) shows the band structure of La_2BaPdO_5. The band gap arises from an indirect transition from the *Z* point to the *R* point of the Brillouin zone. As indicated by the densities of states in La_2BaPdO_5, the bands between −5 and −3.5 eV and −2 eV and E_F have significant Pd 4d character. In La_4LiAuO_8, there is a substantial dispersion of the lowest lying conduction band. In La_2BaPdO_5, however, the lowest energy conduction band is very flat. This is expected considering the molecularity of the PdO_4 units in La_2BaPdO_5, and accounts for the high population of states at the bottom of the conduction band. The small dispersion of this band, corresponding to the Pd $4d_{x^2-y^2}$ orbital, should facilitate partial reduction of Pd^{2+} much more readily than the analogous band in La_4LiAuO_8, which has a dispersion width on the order of 1.5 eV.

The UV−vis spectra of La_4LiAuO_8 and La_2BaPdO_5, obtained from Kubelka−Munk transformation of the diffuse reflectance spectra, are shown in Figure 14. The optical band gap of La_4LiAuO_8 was determined by plotting $[F(R)h\nu]^2$ against $h\nu$, and extrapolating the linear part of the absorption edge to zero. The measured band gap, 3.0 eV, is about 1.1 eV larger than suggested by the DFT-LDA electronic structure. It is well-known that density functional theory with the usual approximations underestimates band gaps, particularly in compounds which do not possess extended networks. Attempts to determine the optical band gap of La_2BaPdO_5 were hindered by the lack of a well-defined (linear) absorbance edge feature in either of the conventional plots of $[F(R)h\nu]^{1/2}$ or $[F(R)h\nu]^{1/3}$ against $h\nu$ for indirect band gap materials. This is in keeping with the band structure which indicates an indirect gap in La_2BaPdO_5.

Catalysis. The catalytic activity of as-prepared and fully reduced La_4LiAuO_8 for CO oxidation was studied in an O_2-rich stream. The temperature-programmed reactions show the expected S-shaped light-off profiles and a regular increase to 100% conversion for both materials, Figure 15. Fully reduced La_4LiAuO_8, with T_{50} = 240 °C, is considerably less active than highly dispersed gold in supported catalysts,[72−74] but the activity is appreciable considering the very low surface area of the reduced material (≈ 3 $m^2\ g^{-1}$) and the large average particle size of Au^0, 43 nm, estimated from Scherrer broadening.

The CO oxidation activity of as-prepared La_4LiAuO_8 is much lower, with T_{50} = 315 °C. Since the as-prepared material does contain some Au^0 on its surface that may contribute to its activity, this result suggests that La_4LiAuO_8 is rather inactive for CO oxidation. The mechanism for CO oxidation over Au/CeO_2 has been proposed

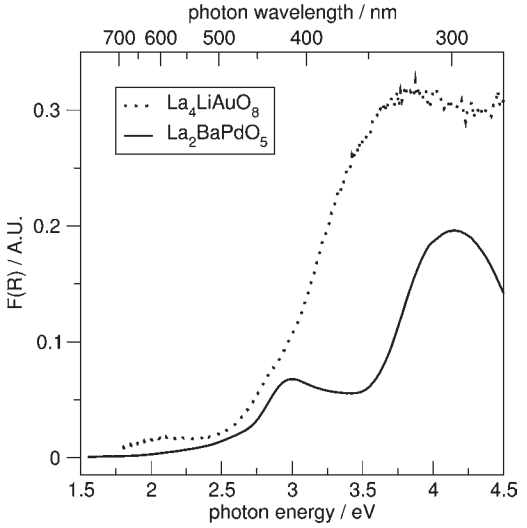

Figure 14. UV−vis spectra of La_4LiAuO_8 and La_2BaPdO_5, obtained from Kubelka−Munk transformation of the diffuse reflectance spectra.

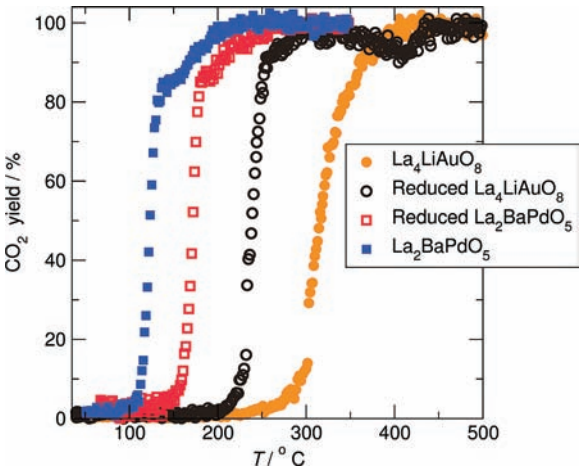

Figure 15. CO-oxidation light-off curves for as-prepared and reduced La_4LiAuO_8 and La_2BaPdO_5.

to involve the ready formation of oxygen vacancies in the CeO_2 support where O_2(g) can be activated.[75,76] In this light, Metiu and co-workers have argued for the role that gold ions play, as substituents in titania[77] and ceria,[78] in activating neigboring oxygen and thereby catalyzing oxidations. La_4LiAuO_8 lacks redox-flexible cations other than Au^{3+}, which is difficult to reduce (as the TGA experiments described above show), and the compound therefore supports few oxygen vacancies. We note that in principle, Au^{3+} compounds could reduce to the intermediate 1+ state during the catalytic process. In the TGA experiments, we noted that somewhat harsh conditions (well above 400 °C in 5%-H_2) are required to reduce La_4LiAuO_8, and in view of this, we do not believe that Au^{1+} species are involved in the catalysis.

(72) Haruta, M. *CATTECH* **2002**, *6*, 102–115.
(73) Miller, J. T.; Kropf, A. J.; Zha, Y.; Regalbuto, J. R.; Delannoy, L.; Louis, C.; Bus, E.; van Bokhoven, J. A. *J. Catal.* **2006**, *240*, 222–234.
(74) Min, B. K.; Friend, C. M. *Chem. Rev.* **2007**, *107*, 2709–2724.
(75) Guzman, J.; Carrettin, S.; Corma, A. *J. Am. Chem. Soc.* **2005**, *127*, 3286–3287.
(76) Camellone, M. F.; Fabris, S. *J. Am. Chem. Soc.* **2009**, *131*, 10473–10483.
(77) Chrétien, S.; Metiu, H. *Catal. Lett.* **2006**, *107*, 143–147.
(78) Shapovalov, V.; Metiu, H. *J. Catal.* **2007**, *245*, 205–214.

The CO oxidation activity of as-prepared and reduced La_2BaPdO_5 was studied under the same conditions. La_2BaPdO_5 is much more active than as-prepared La_4LiAuO_8 for CO oxidation. The as-prepared La_2BaPdO_5 shows high activity at low temperature, with T_{50} = 123 °C. XPS of La_2BaPdO_5 after catalysis showed no change from the as-prepared material, with no discernible contribution from metallic Pd. Similarly, postcatalysis XRD showed single phase La_2BaPdO_5. Unlike reduced La_4LiAuO_8, reduced La_2BaPdO_5 ($\approx$ 5 m^2 g^{-1}) shows lower activity than the as-prepared material for CO oxidation, with T_{50} = 170 °C, although the activity is still significant given the large average particle size of Pd^0, 53 nm. The relatively high activity of the reduced sample could be related to the persistence of oxidized Pd species revealed by XPS.

Recent studies of platinum group metal (PGM) substituted CeO_2 indicate that Pd-substituted materials offer significantly enhanced activity over Pt- or Rh-substituted ceria.[7] It has been shown that an increase in the ionicity of Pd^{2+}, determined from core level XPS binding energies, improves CO oxidation activity.[6] A highly ionic Pd^{2+} environment was identified in Pd-substituted $BaCeO_3$, and it was shown that the aliovalent substitution of Pd^{2+} for Ce^{4+} places the oxygen vacancy required for charge balance adjacent to Pd, leaving it nearly square planar.[70] In the case of $BaCe_{1-x}Pd_xO_{3-\delta}$ ($\delta = x$), it was found that increases in the Pd-substitution level and the corresponding number of vacancies lowered the light-off temperature for CO oxidation.[4] La_2BaPdO_5 similarly contains a highly ionic Pd^{2+} environment with Pd in square planar coordination, but considering its stability toward reduction and the presumable difficulty associated with labilizing lattice oxide in the compound, La_2BaPdO_5 provides an excellent model for examining the mechanism associated with immobilized square planar Pd^{2+} ions that is distinct from one driven by the transport of oxide ions. An in-depth study of the activity of La_2BaPdO_5 is under way.

Conclusions

The quaternary oxide of gold La_4LiAuO_8, and the quaternary oxide of palladium La_2BaPdO_5, are models for investigating the role of cationic metal ions in catalysis, with crystallographically well-defined $Au^{3+}O_4$ and $Pd^{2+}O_4$ square planes. La_4LiAuO_8 can be prepared in air at modest temperatures, and stabilizes the Au^{3+} oxidation state even above 450 °C in 5% H_2. La_2BaPdO_5 stabilizes the Pd^{2+} oxidation state to 550 °C in 5% H_2. The stability of these compounds is attributed to the presence of covalent Au−O and Pd−O bonding as revealed in MEM analysis; such bonding arises from the presence of the highly electropositive countercations. La_2BaPdO_5 is an effective CO oxidation catalyst, and in this, is perhaps the first example of an extended Pd^{2+} oxide with a distinct Pd^{2+} site (as opposed to small substitutions of Pd^{2+} on other cationic sites). It is notable that the crystal structure does not suggest that the catalytic activity is strongly linked to the mobilization of the oxide sublattice, although further investigation is called for. Despite the related crystal structure and the presence of a square-planar d^8 species, La_4LiAuO_8 is *not* an effective catalyst for the reaction studied here. The crucial difference between the two compounds is revealed in DFT electronic structure calculations—filled Au-d states are much deeper in energy that the corresponding Pd-d states, and partial reduction of the metal (for example, Au^{3+} to Au^{2+}) is much harder than the corresponding reduction of palladium because of the smaller population of states at the bottom of the conduction band, and the greater dispersion of the Au $5d_{x^2-y^2}$ orbitals relative to the Pd $4d_{x^2-y^2}$ orbitals. This result, in light of the extensive recent work that has emerged on supported gold particles as catalysts, would suggest that at least in CO oxidation, isolated Au^{3+} ions may not play an important role.

Acknowledgment. We thank the Department of Energy, Office of Basic Energy Sciences for supporting this work through Grant DE-FG02-10ER16081. Use of the Advanced Photon Source was supported by the U.S. Department of Energy, Office of Science, Office of Basic Energy Sciences, under Contract No. DE-AC02-06CH11357. J.A.K. thanks the NSF-PIRE-ECCI (NSF-PIRE-0530268) program for a Studentship during the course of some of this work, and the ConvEne-IGERT Program (NSF-DGE 0801627) for an Associateship. J.A.K. also thanks Jing Huang for her help in the initial stages of this work, and Peter Chupas (APS), Evan Maxey (APS), Katherine Page, and Serena Corr for assistance with the synchrotron data collection. X.O. and S.L.S. acknowledge the donors of the Petroleum Research Fund of the American Chemical Society (ACS-PRF 49221-ND5) for support. W.B.I. is supported by the UCSB Solid State Lighting and Energy Center. We gratefully acknowledge the MRSEC program of the NSF (NSF-DMR 0520415) for facilities.